

# Epigenetic Memory Emerging from Integrated Transcription Bursts

Volker Kurz,<sup>†</sup> Edward M. Nelson,<sup>†</sup> Nicolas Perry,<sup>†</sup> Winston Timp,<sup>‡</sup> and Gregory Timp<sup>†\*</sup>

<sup>†</sup>University of Notre Dame, Notre Dame, Indiana; and <sup>‡</sup>Johns Hopkins University, Baltimore, Maryland

**ABSTRACT** Some autonomous bacteria coordinate their actions using quorum-sensing (QS) signals to affect gene expression. However, noise in the gene environment can compromise the cellular response. By exercising precise control over a cell's genes and its microenvironment, we have studied the key positive autoregulation element by which the *lux* QS system integrates noisy signals into an epigenetic memory. We observed transcriptional bursting of the *lux* receptor in cells stimulated by near-threshold levels of QS ligand. The bursts are integrated over time into an epigenetic memory that confers enhanced sensitivity to the ligand. An emergent property of the system is manifested in pattern formation among phenotypes within a chemical gradient.

## INTRODUCTION

To act in concert, autonomous cells must communicate clearly. Clear lines of communication are vital to a myriad of biological processes in which the signal can affect cell fate, especially in the development and differentiation of cancer cells and immunological response to them (1,2). Noise in the communication channel can compromise the coordination of a communal response, however. Noise is an inherent property of biological signaling, resulting from the small cell volume and stochasticity associated with few copies of genes and dilute concentrations of protein and ligands (3–12). Recent work suggests that biological noise can be filtered and channeled by a signaling network (7), and allows favorable variability in otherwise identical (clonal) cell populations (8), conferring benefits on some phenotypes when subject to sudden environmental changes (9). In particular, a stochastic bistable system is driven by noise instead of being hampered by it. Thus, stochastic bistable switches represent a class of nonlinear systems, which are well suited to adaptation to a fluctuating environment (11,12).

In this article, we examined the effect of noise on cell communication with single cell resolution. We transformed *Escherichia coli* with a gene circuit that leverages a stochastic switching element found in the *lux* operon derived from *Vibrio fischeri*, which has shown positive autoregulation in response to a quorum-sensing (QS) signal 3OC<sub>6</sub>HSL (AHL) (13–16) and (E. Nelson, V. Kurz, N. Perry, D. Kyrouac, and G. Timp, unpublished). Specifically, we leveraged the bidirectional promoter *luxP* in which the left side (*luxP(L)*) controls LuxR production whereas the right (*luxP(R)*) controls production of a degradable variant of green fluorescent protein, GFP-LVA. It has been shown that LuxR positively autoregulates the QS response by modulating its own expression with this switch (14). Bacte-

ria transformed with this stochastic switching element were placed in a stringently controlled microenvironment consisting of a superarray of 3 × 3 arrays of 3 × 3 cells (81 cells in total) using live-cell lithography in a microfluidic device (16) and (E. Nelson, V. Kurz, N. Perry, D. Kyrouac, and G. Timp, unpublished). By patterning cells in this manner, the cellular microenvironment is controlled precisely, allowing each cell to act independently, with access unobstructed by other cells, to the environment. In response to an extracellular signal, transcriptional bursts of receptor production associated with this circuit integrate stochastic noise into a memory invested in LuxR that is retained after cell division, which represents an epigenetic inheritance. Interestingly, an emergent property of this system is spatial pattern formation against a pulsating chemical gradient of the signal in the cell's microenvironment.

Epigenetic inheritance is ubiquitous (17) and it may be possible to harness it to produce predictable biological function. Although the term “epigenetics” typically calls to mind the control of gene expression through DNA methylation, chromatin state, or genetic organization, the definition actually encompasses any heritable change other than in the DNA sequence. This includes the self-sustaining feedback loop described above; the first experimental studies of which involved the bistability of the *lac* operon of *E. coli* (18). Moreover, epigenetic memory like this can confer a survival advantage (19,20). One of the primary advantages of epigenetic gene regulation is the rapidity of switching (19,21). This rapid and increased variation leads to greater fitness—the more variation in phenotype, the better able a population is to survive an unexpected insult or rapid change in the environment (22). Using the bistability of the *lux*-mechanism as a model, we can explore the channeling of noise into epigenetic variations that control and alter the cellular phenotype. Thus, we can illuminate how noise in communication actually confers greater fitness for the bacteria community as a whole.

Submitted April 1, 2013, and accepted for publication August 7, 2013.

\*Correspondence: [gtimp@nd.edu](mailto:gtimp@nd.edu)

Editor: Jason Haugh.

© 2013 by the Biophysical Society  
0006-3495/13/09/1526/7 \$2.00

<http://dx.doi.org/10.1016/j.bpj.2013.08.010>



## MATERIALS AND METHODS

### Bacteria

*Escherichia coli* (DH5 $\alpha$ ) were transformed with the 203 plasmid shown in Fig. S1 in the Supporting Material. The bacteria were grown in M9 (0.2% glycerol) minimal media supplemented with 200  $\mu$ M thiamine and 0.2% (w/v) casamino acids, using kanamycin (50  $\mu$ g/mL) as selection marker. Cultures were incubated at 37°C overnight, diluted 1:10 in fresh media, and harvested when they reached an optical density (OD<sub>600</sub>) of 0.6–0.7.

### Live cell lithography

A microfluidic channel was used to convey the genetically engineered bacteria in a (hydrogel) prepolymer solution to an assembly area where they were subsequently organized into homologous superarrays using optical tweezers and encapsulated in hydrogel. A full description of the optical trapping system is given in Mirsaidov et al. (16). Briefly, bacteria were captured individually and placed into a time-shared array of optical traps using a freely definable shepherd beam. Time-averaged powers in the array and shepherd beam were <1 mW and ~3 mW, respectively. Assembly of each microarray required <1 min. Each superarray was comprised of several regular two-dimensional 3×3 microarrays as illustrated in Fig. S2 a. Adjacent microarrays were spaced 22- $\mu$ m apart (in *X* and/or *Y*).

The hydrogel prepolymer solution consisted of: 3.4 kDa polyethylene glycol diacrylate (PEGDA; Laysan Bio, Arab, AL) at 8% (w/v); M9 (0.2% glycerol); and a photoinitiator, 2-hydroxy-[4-(hydroxyethoxy)]-2-methyl-1-propanone (Irgacure 2959; BASF, Stony Brook, NY) at 0.5% (w/v). The bacteria were centrifuged at 2400 relative centrifugal force for 2.5 min, the supernatant aspirated, and the bacterial pellet resuspended in the prepolymer solution. Cell suspensions were then loaded into 1-mL syringes and injected into microfluidic devices. The prepolymer solution was photopolymerized with 1-s-long exposures using a metal halide light source (X-CITE 120Q; Lumen Dynamics, Mississauga, Ontario, Canada) and a 370  $\pm$  25-nm bandpass UV filter (Semrock, Rochester, NY), yielding 75 mW/cm<sup>2</sup> at the objective. A square mask (~5.0 × 5.0 mm) placed in front of the UV source was used to control the shape and size of the hydrogel spot.

### Confocal microscopy

The fluorescence data were collected using a TCS SP5 II (Leica, Mannheim, Germany) confocal microscope with enhanced, hybrid *GaAsP* detectors for improved sensitivity to fluorescence. All confocal images were acquired using a 100×, 1.44 NA oil immersion objective with an argon laser excitation (488 nm) at 500 nW using a 147.5- $\mu$ m pinhole (1 Airy unit). Correspondingly, each voxel has a width and height of 178.4 nm and a depth of 377.7 nm for a total volume of 12,020,891 nm<sup>3</sup> or  $V_c = 12.0 \times 10^{-18}$  L = 12 aL. Each image was acquired at a 8-kHz line rate using eight line accumulations. Each voxel was exposed for 125 ns for a total excitation exposure time per voxel of 1.0  $\mu$ s. Fluorescent z-stacks (along the optic axis) were recorded every 10 min. Around each bacterium, a 5- $\mu$ m square-shaped region-of-interest (ROI) was defined and the mean intensity in each time-lapse maximum projection image extracted, yielding time-intensity plots called kymographs. False-color perspective volumes were reconstructed from image stacks (Bitplane, Zurich, Switzerland) obtained from a series of confocal images, and then a contour defining that volume was defined by selecting an individual voxel and searching all surrounding voxels for similar intensity.

### Stochastic simulations

The complex processes underpinning LuxR and GFP production, gene transcription, and mRNA translation were assembled into the model represented in Fig. 1, a and b, using the kinetic rate constants delineated in Table 1. The constitutive production of LuxR (species *R*) was modeled

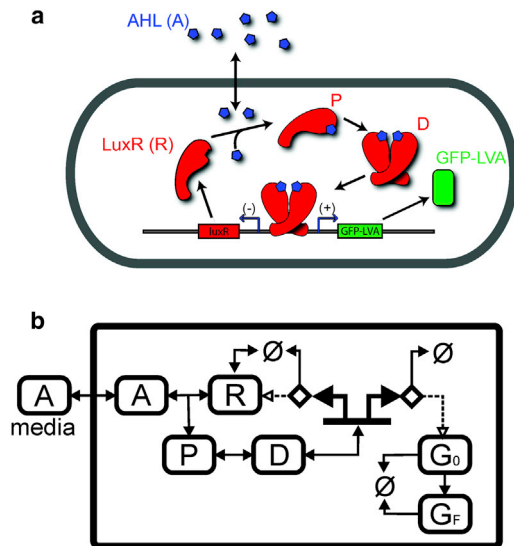


FIGURE 1 (a) Schematic model of the LuxR-bistable switch and (b) the corresponding detailed model of the operation of the switch used for stochastic simulations. The species *A* is the autoinducer AHL, which diffuses into and out of the cell; *R* is LuxR; *P* is the LuxR/AHL complex; *D* is dimerized *P*; and  $G_0$  and  $G_F$  are nonfluorescent and fluorescent GFP-LVA, respectively. ( $\diamond$ ) mRNA; ( $\emptyset$ ) degradation/basal production.

as a first-order catalytic reaction. Its degradation occurs primarily via dilution through cell proliferation, which is measured by the doubling-time  $\lambda_0$ . The AHL inducer (species *A*) binds with LuxR to form the product *P* in a second-order kinetic reaction. According to Fig. 1 b, *P* then dimerizes to form *D* in another second-order reaction. Thus, the production of *R*, *P*, and *D* were modeled by the following reactions and reaction rates (in brackets):

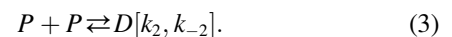
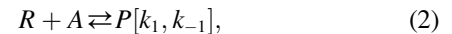


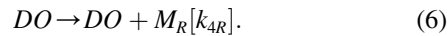
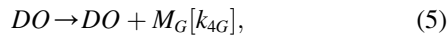
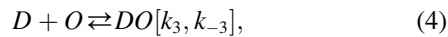
TABLE 1 Kinetic rate constants used in the model

Symbol	Value	Units <sup>a</sup>	Description
$k_0$	$3 \times 10^{-4}$	$m s^{-1}$	Constitutive production of <i>R</i>
$k_1$	$1.4 \times 10^{-4}$	$m^{-1} s^{-1}$	Association between <i>R</i> and <i>A</i>
$k_{-1}$	$3.33\text{--}4.3 \times 10^{-3}$	$s^{-1}$	Dissociation of <i>P</i>
$k_2$	$3 \times 10^{-5}$	$m^{-1} s^{-1}$	Dimerization of <i>P</i>
$k_{-2}$	$1\text{--}1.2 \times 10^{-2}$	$s^{-1}$	Dissociation of <i>D</i>
$k_3$	$2 \times 10^{-3}$	$m^{-1} s^{-1}$	Binding of <i>D</i> and Operator
$k_{-3}$	$1 \times 10^{-2}$	$s^{-1}$	Dissociation of <i>DO</i>
$k_{4G}$	$1.4 \times 10^{-2}$	$s^{-1}$	Transcription of GFP-LVA mRNA
$k_{4R}$	$1.4 \times 10^{-4}$	$s^{-1}$	Transcription of <i>luxR</i> mRNA
$k_{5G}$	$6.4 \times 10^{-2}$	$s^{-1}$	Translation of GFP-LVA mRNA
$k_{5R}$	$6.0 \times 10^{-2}$	$s^{-1}$	Translation of <i>luxR</i> mRNA
$k_6$	$7.2\text{--}9 \times 10^{-4}$	$s^{-1}$	Oxidation of GFP-LVA
$\lambda_0$	$8.8 \times 10^{-5}$	$s^{-1}$	Degradation of LuxR
$\lambda_1$	$1 \times 10^{-3}$	$s^{-1}$	Degradation of mRNA
$\lambda_2$	$5\text{--}6 \times 10^{-4}$	$s^{-1}$	Degradation of GFP
$k_D$	0.23	$s^{-1}$	Diffusion of <i>A</i>

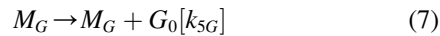
Model used was from Goryachev et al. (15).

<sup>a</sup>Molecules/cell is abbreviated *m*.

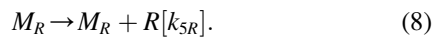
The dimer  $D$  binds to the operon (species  $O$ ) and initiates transcription of mRNA ( $M$ ). This was captured by the following kinetic reactions:



Translation of mRNA into GFP-LVA ( $G_0$ ) and  $R$  was modeled by the following first-order reactions:



and



Oxidation of GFP (species  $G_F$ ) and degradation of GFP and mRNA were modeled by first-order kinetics given by



Exogenously applied AHL diffuses through the cell wall and was described by the reaction



To account for cell division, the number of cells is doubled and the number of species in each cell is reduced by half every  $\lambda_0 = 185 \pm 10$  min, where  $\lambda_0$  the doubling time, while keeping track of the total number of species divided between daughter cells. The number of species in each cell was calculated from macroscopic quantities by taking into account the measured volume of the cell: 1 molecule per cell corresponds to  $\sim 1/(V \times N_A) = 1.7$  nM, where  $N_A$  is Avogadro's number. The initial amount of LuxR in the system was a normally distributed random number  $R_0$  (mean 50, standard deviation 10). The initial number of DNA plasmids ( $O$ ) was set to  $O = 10$  for low-copy plasmids. External AHL ( $A_{ex}$ ) was treated as a boundary condition and was not varied in the simulation, but depends on the flow conditions imposed on the cells in the experiment. The dynamic behavior of each state vector was simulated using Gillespie's algorithm (23) in MATLAB (Ver. 2012a; The MathWorks, Natick, MA). Because stochastic simulations rely on an element of probability, we used multiple stochastic runs to account for fluctuations in the behavior of the model.

## RESULTS

We assert that biological noise can be channeled using a bistable element like that found in the *lux* operon shown in Fig. 1, allowing phenotypes to develop in a clonal cell population that favor a microenvironment with QS signals in it. To prove this assertion, we utilized the 203 plasmid (see Fig. S1) consisting of a fragment of the *lux* operon: the *luxP(L)* promoter controlling LuxR production and the *luxP(R)* promoter controlling the production of a degradable variant of green fluorescent protein, GFP-LVA (24). A cell

population transformed with this system, LuxR, which is constitutively expressed at a low level, is upregulated twofold by AHL induction for concentrations  $>2$  nM, as we demonstrated using RT-qPCR (see Fig. S3), which is consistent with prior work (14). Different levels of LuxR protein provide different responses to AHL within the same cell population or even the same cell, which were evident in laser cytometry data (E. Nelson, V. Kurz, N. Perry, D. Kyrouac, and G. Timp, unpublished) and the hysteresis shown in the Supporting Material (see Fig. S4) and elsewhere (14). Fig. S4 shows a history-dependent, hysteretic graph of the fluorescence obtained from a single cell/microcolony (within a superarray of 54 cells) to a slowly varying fluctuating stimulus. When the concentration of AHL in the cellular microenvironment was modulated, starting at 0 nM AHL and stepping in 1-nM increments to 10 nM and then returned to 0 nM over 12 h, the fluorescence showed a hysteretic response that was indicative of memory. To understand the role LuxR plays in the memory, the concentration of LuxR and the expression of GFP were simulated stochastically using the model described in Fig. 1. The simulations, which mirrored the conditions used in the experiment along with the experimental data, indicate that single cells transformed with this gene circuit exhibit bistability between LOW and HIGH LuxR states in a static environment with a bifurcation starting near 2–3 nM AHL, which lends further support to the idea of positive LuxR transcriptional autoregulation (14).

Fig. 2, *a* and *b*, shows the time development over 6 h of the fluorescence of a single element in a superarray of 81 homologous bacteria immersed in a static environment containing 3 nM AHL. The concentration of AHL is uniform with  $<1\%$  variation throughout the array within  $\sim 1.5$  min after a 100- $\mu$ L/min flush (see Fig. S2 *b* and (E. Nelson, V. Kurz, N. Perry, D. Kyrouac, and G. Timp, unpublished)), yet the cells in Fig. 2 *a* appear to blink repeatedly on-and-off again over  $\sim 120$  min (25). Out of the 81 cells in the array, 27 (33%) demonstrated this behavior, whereas 33 (41%) were in the HIGH state and 21 (26%) were in the LOW state. In contrast, at 100 nM AHL the fluorescence increases monotonically (Fig. 2, *d* and *e*), which is consistent with cells in either a HIGH or LOW state responding to this saturating condition by inducing the HIGH expression state in the population. The data of Fig. 2 *a* are inconsistent with either photobleaching or on-off blinking of fluorescence observed in single molecule studies of GFP mutants (26–28) (see Fig. S5 and Fig. S6). The measured fluorescent lifetime of GFP in these cells is 790 ms, which rules out photobleaching for the imaging conditions used here. In addition, with an absorption rate of 25 photons per GFP molecule and an excitation cross-section of  $2 \times 10^{-16}$  cm<sup>2</sup>, these results exclude conventional GFP blinking (30). Instead, we propose that this blinking is a result of transcriptional bursting, the subsequent degradation of GFP-LVA, and the resulting fluctuations in the number of GFP-LVA molecules.

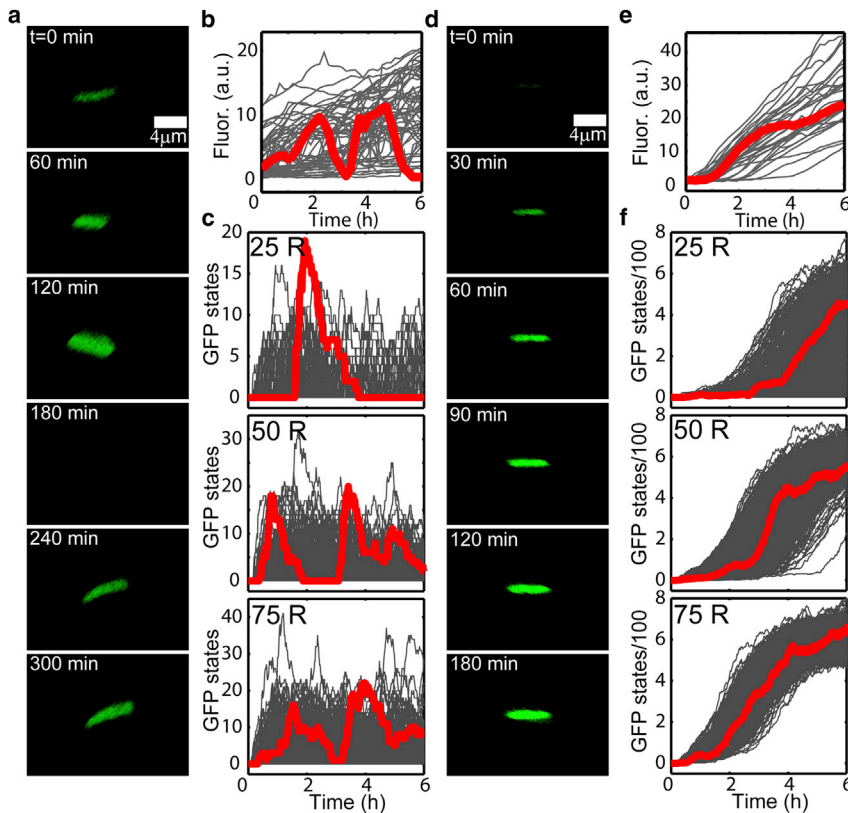


**FIGURE 2** (a) Fluorescent confocal microscopy illustrating transcriptional bursting at 3 nM AHL. GFP-LVA is expressed, making the bacteria fluoresce, and then degraded due to the LVA tag, resulting in a loss of fluorescence. Two blinks are shown. (b) Time evolution of the total fluorescence associated with a typical cell in panel *a* is highlighted (red), with the response of 60 other cells to the same experimental conditions also highlighted (gray). (c) Stochastic simulations showing the evolution of GFP-LVA with three molecules of extracellular AHL. The cells are initialized with 25, 50, or 75 LuxR (R) molecules. (Red) Typical response from one cell out of 1000. (d) Like panel *a*, but for 100 nM AHL. (e) Like panel *b*, the evolution of the fluorescence associated with a single cell represented in panel *d* is highlighted (red), with the response of 30 other cells to the same conditions also highlighted (gray). (f) Like panel *c*, stochastic simulations showing the time evolution of GFP-LVA at 100 molecules of extracellular AHL.

We used the characteristics of the transcription bursts to infer information about the LuxR concentration through stochastic simulations. Drawing the parameters that govern the reaction kinetics of LuxR from Goryachev et al. (15), the single cell fluorescence data were simulated using the model in Fig. 1. This model accurately captures the transcription and translation of both LuxR and GFP-LVA in each cell. For example, independent stochastic simulations of an ensemble of 10,000 cells, initialized with 50 LuxR molecules per cell, indicates a bifurcation threshold for AHL concentrations between 1 and 2 molecules per cell. For extracellular concentrations of AHL  $>2$  molecules, the cells switch to the HIGH expression state based on the number of fluorescent GFP molecules in the system, in agreement with cytometry measurements and (E. Nelson, V. Kurz, N. Perry, D. Kyrouac, and G. Timp, unpublished). According to the simulation, positive autoregulation produces bistability at an AHL concentration near two molecules of extracellular AHL per cell or  $\sim 3$  nM.

Fig. 2 *c* shows the simulated time evolution of GFP-LVA for 100 cells out of an ensemble of 1000 cells with 25, 50, or 75 initial LuxR molecules per cell and three molecules of extracellular AHL per cell. A single representative cell was selected and plotted in red for clarity. If the initial concentration was 25 LuxR molecules in a cell, then 5% of the cells in the ensemble would blink, whereas the majority (69.8%) would remain in the LOW state, defined as having  $<5$  molecules of GFP-LVA per cell. On the other

hand, if the initial number of LuxR molecules was 50 per cell, then 22.4% of the cells would blink, whereas 25.4% would remain in the LOW state, which compares favorably to the experimental data. Lastly, if there were 75 molecules of LuxR, 52.8% of the cells would blink, but only 5.3% were found to be in the LOW state. By comparing the fractional population that blinks, switched to HIGH or remained LOW with the experimental data, we concluded that each cell had  $\sim 50$  LuxR initially. Consequently, all subsequent simulations were initialized with  $50 \pm 10$  LuxR molecules. Finally, for cells with a starting concentration of  $50 \pm 10$  LuxR molecules, we estimate that the mean number of LuxR molecules in a cell is  $\sim 140$  after 6 h of exposure to 3 nM AHL. Thus, LuxR accumulates in the cell with continuous exposure to AHL even if GFP-LVA degrades.

The delicate balance between GFP-LVA production and proteolytic digestion produces bursts of fluorescence. From the model, we infer that LuxR is also produced in bursts, but unlike GFP-LVA, it accumulates in the cells as it degrades only by dilution through cell proliferation (E. Nelson, V. Kurz, N. Perry, D. Kyrouac, and G. Timp, unpublished). In contrast with the 3-nM exposure, in 100 nM AHL, GFP-LVA (and by inference, LuxR) is produced at so high a rate as to be practically continuous, thus leading to the monotonic increase in fluorescence shown in Fig. 2 *e*. The simulations in Fig. 2 *f* with 25, 50, and 75 initial LuxR molecules are all consistent with this behavior. All the simulations indicate the mean number of LuxR in each

microcolony grows to  $>970$  molecules (in each cell the number grows to  $>485$  molecules) after the initial 6 h exposure to 100 nM AHL, which gives rise to persistent memory as the mean doubling time for the 203 bacteria is 190 min (E. Nelson, V. Kurz, N. Perry, D. Kyrouac, and G. Timp, unpublished). Taken together, the data support the idea that the luxP promoter is a stochastic bistable element that is sensitive to the examined environment and its history.

Memory is a property of bistable biochemical systems like this (1). The memory in this system is invested in the concentration of LuxR in each cell (14) and (E. Nelson, V. Kurz, N. Perry, D. Kyrouac, and G. Timp, unpublished). The concentration of LuxR affects the sensitivity of the bacteria to AHL exposure. High levels of LuxR allow the bacteria to respond to lower levels of AHL with upregulation (HIGH state), whereas cells with low levels of LuxR are unresponsive without higher levels of AHL (LOW state). Changes in the memory status can occur either through production of LuxR via induction with AHL (LOW  $\rightarrow$  HIGH) or via dilution of the LuxR over time through cell division (HIGH  $\rightarrow$  LOW).

This memory can affect the spatial organization of phenotypes. To demonstrate this, we stitched together 22 (of which 17 showed some response to AHL)  $3 \times 3$  arrays of 203 bacteria into a superarray that spanned the width of a  $426\text{-}\mu\text{m}$ -wide microfluidic channel. The microfluidic device has multiple inlet ports, which allows a chemical gradient to be established in the channel. Fig. 3 *a* depicts finite element simulations of the resulting 0–10 nM AHL gradient across the channel, whereas Fig. 3 *b* shows the corresponding fluorescent and optical micrographs of the superarray spanning the channel. The bacteria were repeatedly exposed to the chemical gradient for 60 min followed by flushing for 120 min with no ligand, thus imitating a periodically fluctuating environment.

Fig. 3, *c* and *d*, illustrates an emergent property of the memory invested in LuxR that develops with repeated exposure to the QS signal: i.e., memory translates to spatial pattern development of the phenotypes. Around each bacterium, a  $15\text{-}\mu\text{m}$  square-shaped ROI was defined from which the mean intensity was extracted. The spatial development and time evolution of the GFP-LVA expression was then measured for 17 ROIs spanning the AHL gradient and captured in the so-called kymographs shown in Fig. 3, *c* and *d*. Initially, the arrays among ROI 1–7 (9.5–10.0 nM) showed strong fluorescence as evident in Fig. 3 *c* whereas cells in arrays 8–16 (1–9.5 nM) fluoresce only sporadically, and ROI 17 ( $<1$  nM) showed no fluorescence at all because the bifurcation threshold of 1 nM was positioned at array 16, this is consistent with laser cytometry results (E. Nelson, V. Kurz, N. Perry, D. Kyrouac, and G. Timp, unpublished). After repeated pulses, the spatial response sharpened as the cells in the sporadic regime integrated transcriptional bursts, resulting in a shift to the more-sensitive HIGH state. The effect of noise on gradient sensing was thus ameliorated

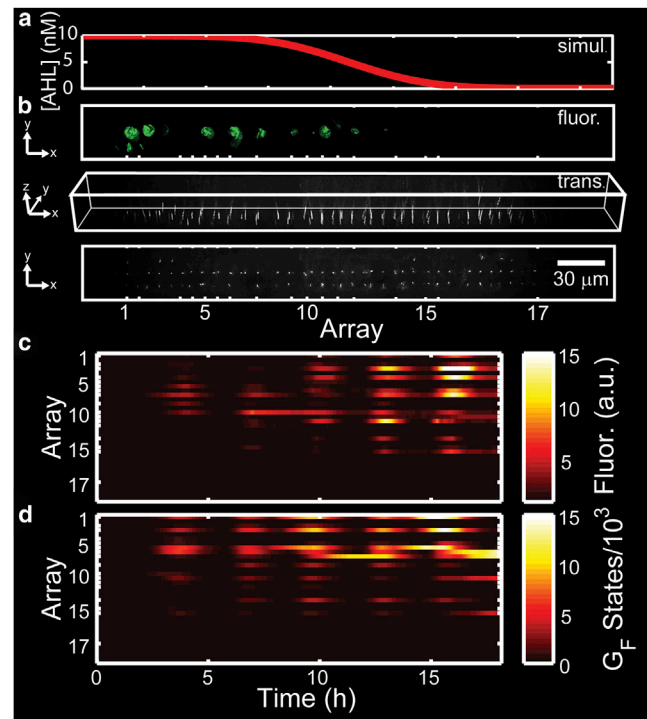


FIGURE 3 (a) Finite element model of the AHL gradient in the channel matching the experiment. (b) A linear array of 203s spanning the width of a microfluidic channel where an AHL concentration gradient is established. (From top to bottom) Fluorescence (at 16 h) and transmission images (side-view and top-down) of a linear superarray of  $1.7\text{--}3 \times 3$  microarrays, constructed midway down the length of a  $3600\text{-}\mu\text{m}$ -long microfluidic channel to span the entire  $426\text{-}\mu\text{m}$  width of the channel. (c) Kymograph showing the time evolution of the fluorescence in the 17 ROIs from panel *b*. (d) Stochastic simulation showing the ensemble (nine cells) average of GFP production corresponding to conditions in panels *a* and *b*.

by the memory invested in LuxR—and the receptor production integrated over time leads to more sensitivity to the ligand, producing a sharper detection threshold. The corresponding stochastic simulations of a nine-cell ensemble shown in Fig. 3 *d* demonstrated similar pattern formation. From the simulations, it was concluded that stochastic variation was diminished as receptor production was integrated over time, leading to more sensitivity to the ligand and producing a more-sensitive detection threshold than would be assumed from the bulk response. This result demonstrates that the memory of the system and its ability to integrate over history allows the cell to properly respond to long timescale signals by showing a sharp threshold of phenotype. So, the system grants a heterogeneous response to transient signals and adapts to persistent signals, resulting in alterations in the population's phenotype distribution.

## DISCUSSION

We have studied a key stochastic switching element found in the lux QS system, a bidirectional promoter luxP, that has

shown positive autoregulation in response to a QS signal AHL. By exercising precise control over the gene's microenvironment, we established that the autoregulation of the Lux receptor provides a memory for the system, increasing the sensitivity and removing variability via accumulation of the receptor protein. The memory that is invested in LuxR depends on the initial exposure and degrades only by cell proliferation. It persists for several generations, even in the absence of the QS signal (E. Nelson, V. Kurz, N. Perry, D. Kyrouac, and G. Timp, unpublished), and so it represents an epigenetic inheritance. This retained epigenetic memory allows for phenotypic inheritance, while providing a minimal level of signal response. Feedback is necessary for this behavior, as it is not present in the lac repressor system (LacI) alone (14).

This system provides a model to address two key questions:

1. Why and where within a population of bacteria will some individuals express a gene, whereas genetically identical neighbors do not?
2. Under what conditions, and for how long, do the epigenetic variants persist?

To answer these questions, we used live cell lithography to place a superarray like that shown in Fig. 3 in a ligand gradient. When placed in a gradient, the cell population's reaction ranges from no (LOW) response to full (HIGH) LuxR response. The effect of noise in gradient sensing is ameliorated by the attained memory-receptor production, which is integrated over time, leading to more sensitivity to the ligand. This produces a sharper detection threshold than would be assumed from the noisiness observed in a bulk response with consequences for pattern formation, for example (30). Essentially, both a graded or analog response and a digital or binary response are possible with the same system (31). By applying a short pulse of ligand to a naïve system, cells in the bistable regime, on average, will give intermediate levels of response. However, after a larger dosage or multiple short doses of ligand, the receptor levels will rise, resulting in an all-or-nothing response, as we have shown. In particular, Fig. 3, *c* and *d*, shows that after three 1-h pulses of AHL at a concentration in the range 9.5–10 nM, the HIGH expression state was induced and persisted. On the other hand, cells exposed to AHL concentrations in the range 1–9.5 nM are forced to HIGH state expression reluctantly. Only after exposure to five-1 h pulses of AHL at a concentration of ~1 nM is the HIGH expression state induced.

Thus, owing to the memory of fluctuations in a precisely controlled environment, heritable variations in gene expression create phenotype diversity within an isogenic population of bacteria. The phenotype diversity in the population is manifested in exposure to a short-term stimulus (such as a pulse of AHL at low concentration.) This promotes a

maximally fit population. On the other hand, persistent exposure to AHL removes phenotype diversity with the majority of the cells transforming to the HIGH state. Thus, the memory allows both adaptation to persistent changes in environment and the ability to respond to short-term changes via diversity of phenotype. Epigenetic memory like this could bestow a fitness advantage affecting, for example, the evolution of antibiotic resistance (19) or even bacterial-induced regulation of host cell function in bacterial infections (20). In particular, it has been observed that a colony of cells carrying a plasmid conferring antibiotic resistance reduces the concentration of antibiotic in the immediate neighborhood, producing a gradient that facilitates the survival of other cells surrounding the resistant colony (19). Although there may be a large number of cells surrounding the resistant colony, only a few of these form satellites. So, why would these few cells grow rather than die? The data is not consistent with DNA mutation. Rather, it has been posited that heritable epigenetic variation creates a phenotypic diversity susceptible to natural selection (20). Our data are consistent with this interpretation.

Thus, the stringent control over the cell's genes and its microenvironment offered by this simple model allows for unequivocal tests of hypotheses, especially those related to gradients in nutrients or environmental signals that might affect phenotype development. However, the interactions found in nature are often more complex than a single species on a hydrogel scaffold in a two-dimensional synthetic biofilm such as this can mimic. To accommodate natural complexity, the methods used to construct this model can be extended to incorporate multiple species into three-dimensional architectures with open channels that are more reminiscent of native biofilms (32). Furthermore, the observed bistability and resulting gradient induced spatial organization is important not just in bacteria, but has implications for eukaryotic development as well. During development, cells integrate signals in their environment into an epigenetic memory, inducing different phenotypes (33). The epigenetic state is then regulated by various feedback loops forcing the expression of one set of genes whereas others remain silent (34). It also has implications for biocomputing (35), because it could help to define the layout and timing conditions necessary for sequential logic. In particular, a sequential logic network merges combinatorial logic (36), in which the output is purely a function of the input, with information storage devices (like a bistable multivibrator, i.e., a flip-flop) to produce a network that receives an input and produces an output that is a function of both the examined input and its history. The time development of the memory and the position of the boundary observed in this gradient define line rules required to lay out logical elements in a sequential network and the minimum settling time before the output can be read out.

## CONCLUSIONS

We have studied a bistable switching element inherent to the *lux* QS system that integrates noisy signals into an epigenetic memory by exercising precise control over a cell's genes and its microenvironment. We observed transcriptional bursting of the *lux* receptor in cells stimulated by near-threshold levels of QS ligand. The bursts are integrated over time into an epigenetic memory that confers enhanced sensitivity to the ligand. An emergent property of the system is manifested in pattern formation among phenotypes within a chemical gradient. Thus, by using live cell lithography in combination with a microfluidic device to control the microenvironment of individual cells in a population, models like this and the patterns they produce could be used to illuminate the answers to key questions in development.

## SUPPORTING MATERIAL

Six figures are available at [http://www.biophysj.org/biophysj/supplemental/S0006-3495\(13\)00923-5](http://www.biophysj.org/biophysj/supplemental/S0006-3495(13)00923-5).

We are grateful to R. Weiss for the donation of 203 plasmid.

We acknowledge support from National Science Foundation grants No. CCF-1129098.

## REFERENCES

- Xiong, W., and J. E. Ferrell, Jr. 2003. A positive-feedback-based bistable 'memory module' that governs a cell fate decision. *Nature*. 426:460–465.
- Cotari, J. W., G. Voisinne, ..., G. A. Bonnet. 2013. Cell-to-cell variability analysis dissects the plasticity of signaling of common G chain cytokines in T cells. *Sci. Signal*. 6:266.
- Spudich, J. L., and D. E. Koshland, Jr. 1976. Non-genetic individuality: chance in the single cell. *Nature*. 262:467–471.
- Berg, H. C., and E. M. Purcell. 1977. Physics of chemoreception. *Biophys. J.* 20:193–219.
- Elowitz, M. B., A. J. Levine, ..., P. S. Swain. 2002. Stochastic gene expression in a single cell. *Science*. 297:1183–1186.
- Isaacs, F. J., J. Hastly, ..., J. J. Collins. 2003. Prediction and measurement of an autoregulatory genetic module. *Proc. Natl. Acad. Sci. USA*. 100:7714–7719.
- Cheong, R., A. Rhee, ..., A. Levchenko. 2011. Information transduction capacity of noisy biochemical signaling networks. *Science*. 334:354–358.
- Munsky, B., G. Neuert, and A. van Oudenaarden. 2012. Using gene expression noise to understand gene regulation. *Science*. 336:183–187.
- Thattai, M., and A. van Oudenaarden. 2004. Stochastic gene expression in fluctuating environments. *Genetics*. 167:523–530.
- Blake, W. J., G. Balázsi, ..., J. J. Collins. 2006. Phenotypic consequences of promoter-mediated transcriptional noise. *Mol. Cell*. 24:853–865.
- Raser, J. M., and E. K. O'Shea. 2005. Noise in gene expression: origins, consequences, and control. *Science*. 309:2010–2013.
- Rao, C. V., D. M. Wolf, and A. P. Arkin. 2002. Control, exploitation and tolerance of intracellular noise. *Nature*. 420:231–237.
- Miller, M. B., and B. L. Bassler. 2001. Quorum sensing in bacteria. *Annu. Rev. Microbiol.* 55:165–199.
- Williams, J. W., X. Cui, ..., A. M. Stevens. 2008. Robust and sensitive control of a quorum-sensing circuit by two interlocked feedback loops. *Mol. Syst. Biol.* 4:234.
- Goryachev, A. B., D. J. Toh, and T. Lee. 2006. Systems analysis of a quorum sensing network: design constraints imposed by the functional requirements, network topology and kinetic constants. *Biosystems*. 83:178–187.
- Mirsaidov, U., J. Scrimgeour, ..., G. Timp. 2008. Live cell lithography: using optical tweezers to create synthetic tissue. *Lab Chip*. 8:2174–2181.
- Jablonka, E., and G. Raz. 2009. Transgenerational epigenetic inheritance: prevalence, mechanisms, and implications for the study of heredity and evolution. *Q. Rev. Biol.* 84:131–176.
- Novick, A., and M. Weiner. 1957. Enzyme induction as an all-or-none phenomenon. *Proc. Natl. Acad. Sci. USA*. 43:553–566.
- Adam, M., B. Murali, ..., S. S. Potter. 2008. Epigenetic inheritance based evolution of antibiotic resistance in bacteria. *BMC Evol. Biol.* 8:52.
- Bierne, H. M., M. Hamon, and P. Cossart. 2012. Epigenetics and bacterial infections. *Cold Spring Harb. Perspect. Med.* 2:a010272.
- Rando, O. J., and K. J. Verstrepen. 2007. Timescales of genetic and epigenetic inheritance. *Cell*. 128:655–668.
- Feinberg, A. P., and R. A. Irizarry. 2010. Evolution in health and medicine Sackler colloquium: stochastic epigenetic variation as a driving force of development, evolutionary adaptation, and disease. *Proc. Natl. Acad. Sci. USA*. 107(Suppl 1):1757–1764.
- Gillespie, D. T. 1977. Exact stochastic simulation of coupled chemical reactions. *J. Phys. Chem.* 81:2340–2361.
- Andersen, J. B., C. Sternberg, ..., S. Molin. 1998. New unstable variants of green fluorescent protein for studies of transient gene expression in bacteria. *Appl. Environ. Microbiol.* 64:2240–2246.
- Cai, L., N. Friedman, and X. S. Xie. 2006. Stochastic protein expression in individual cells at the single molecule level. *Nature*. 440:358–362.
- Creemers, T. M. H., A. J. Lock, ..., S. Völker. 2000. Photophysics and optical switching in green fluorescent protein mutants. *Proc. Natl. Acad. Sci. USA*. 97:2974–2978.
- Dickson, R. M., A. B. Cubitt, ..., W. E. Moerner. 1997. On/off blinking and switching behavior of single molecules of green fluorescent protein. *Nature*. 388:355–358.
- Kubitschek, U., O. Kückmann, ..., R. Peters. 2000. Imaging and tracking of single GFP molecules in solution. *Biophys. J.* 78:2170–2179.
- Peterman, E. J. G., S. Brasselet, and W. E. Moerner. 1999. The fluorescence dynamics of single molecules of green fluorescent protein. *J. Phys. Chem. A*. 103:10553–10560.
- Basu, S., Y. Gerchman, ..., R. Weiss. 2005. A synthetic multicellular system for programmed pattern formation. *Nature*. 434:1130–1134.
- Biggar, S. R., and G. R. Crabtree. 2001. Cell signaling can direct either binary or graded transcriptional responses. *EMBO J.* 20:3167–3176.
- Akselrod, G., W. Timp, ..., G. Timp. 2006. Laser-guided assembly of living cell microarrays. *Biophys. J.* 91:3465–3473.
- Reik, W., W. Dean, and J. Walter. 2001. Epigenetic reprogramming in mammalian development. *Science*. 293:1089–1093.
- Demongeot, J., M. Kaufman, and R. Thomas. 2000. Positive feedback circuits and memory. *C. R. Acad. Sci. III*. 323:69–79.
- Bray, D. 1995. Protein molecules as computational elements in living cells. *Nature*. 376:307–312.
- Daniel, R., J. R. Rubens, ..., T. K. Lu. 2013. Synthetic analog computation in living cells. *Nature*. Published online:1476–4687.